DOI: https://doi.org/10.1051/e3sconf/202016800003

GEOELECTRICAL TOMOGRAPHY DATA PROCESSING AND INTERPRETATION FOR PB-ZN-AG MINERAL EXPLORATION IN NASH CREEK, CANADA

[1,2]Mosaad Ali, [1]Shulin Sun, [1]Wei Qian, [1]Abdou Dodo Bohari, [1]Dusabemariya Claire, [1]Yan Zhang

[1]School of Earth Science and Engineering at Hohai University, [2]Mining and Metallurgical Engineering Department at Assiut University

Abstract. The geoelectrical tomography survey was carried out to explore and characterize a (Zn-Pb-Ag) sulphide deposit in Nash Creek (NC), New Brunswick province, Canada. The exploration strategy has been conducted by the 2-D survey for a well-cut grid consisting of twelve surface lines (profiles) each around 2 km long, and 300 m apart, for the total area around 9.5 km^2. The datasets (resistivity and induced polarization) were acquired using the Iris El-Rec Pro system with pole-dipole electrodes array spaced 50 m apart, and ten levels of data datum. The results of the 2-D inversion revealed that the underground resistivity and chargeability values in the exploration area have a range of (5 to 1300 Ωm) and (0-9.5 mV/V), respectively. The sulphide mineralization zones in the exploration area are characterized by moderate resistivity values (150-300 Ωm) and moderate to low chargeability values (>5.5 mV/V), with a depth of around (90-140 m) from the surface. The 3-D visualization model clearly reveals that three main zones of sulphide mineralization are present in the exploration area. The predicted geological reserve of the sulphide ore in the exploration area was calculated. The inverted models revealed a good agreement with the existing geological features in the exploration area.

Introduction. Exploring underground minerals on the surface is a significant challenge. Because of the mineral deposits are usually existed in geologically complex formations and associated with the host rocks, so it is hard to distinguish. Especially, to identify mineralization zones with a low-grade ore. One of the geophysical techniques that can be applied effectively for that is the geoelectrical technique (DCIP) (direct current (DC) resistivity and induced polarization (IP)) [1–3]. This technique produces two parameters, namely resistivity and chargeability, which quite well distinguishes the mineral deposit content in rocks [4–6]. The DCIP technique has demonstrated to be a useful and effective tool in the exploration of mineral resources (metallic and non-metallic) [7–10]. Especially, the IP method is widely used for mineral exploration because it is the only geophysical technique that has the ability to discriminate conductive or semi-conductive minerals disseminated in high electrical resistivity background (host rock) [11–14].

In this work, we present the results of the 2-D geoelectrical survey from the Nash Creek (NC) (Zn-Pb-Ag) sulphide deposit. The NC deposit is found along the western edge of the Jacquet River Graben in NE New Brunswick province, Canada. The metal sulphides are considered as the most important group of ore minerals for most of the world supplies of non-ferrous metals [15]. The sulphide mineralized environments are described by strong clay alterations and carbonization [16]. At the study area, widespread brecciation units and alteration zones (associated typically with a pyrite-rich accumulation) pose a problem for traditional electromagnetic exploration methods where low-grade sulphides are imbedded in laterally wide alteration envelopes [17, 18].

In order to produce proper exploration methodology for the NC deposit, the DCIP datasets were acquired using the Iris El-Rec Pro system with a pole-dipole electrodes

array to find out the distribution of mineralized zones and underground formation description of the massive sulphide deposits based on resistivity and chargeability values. The DCIP datasets of this survey have been described and analysed using RES2DINV ver. 4.8.10 software trial version of the 2-D inversion carried out based on the finite element method [19, 20]. Also, the 3-D view of the inverted datasets was carried out to assist in the interpretation, using Golden Software Voxler 4.

Inversion results have confirmed to provide the accurate spatial agreement of the information collected by the DCIP survey; this makes the geoelectrical tomography a valuable exploration tool for mineral exploration even with low-grade ores. The inverted models revealed a good agreement with the existing geological features in the exploration area. The study recommends that if pre-existing information regarding the geological environment is available, then geoelectrical tomography data (resistivity and changeability) can be a helpful and fascinating mixture for mineral exploration.

Location and Geology. The NC area is found along the western edge of the Jacquet River Graben in NE New Brunswick province, Canada, in Figure 1-a.

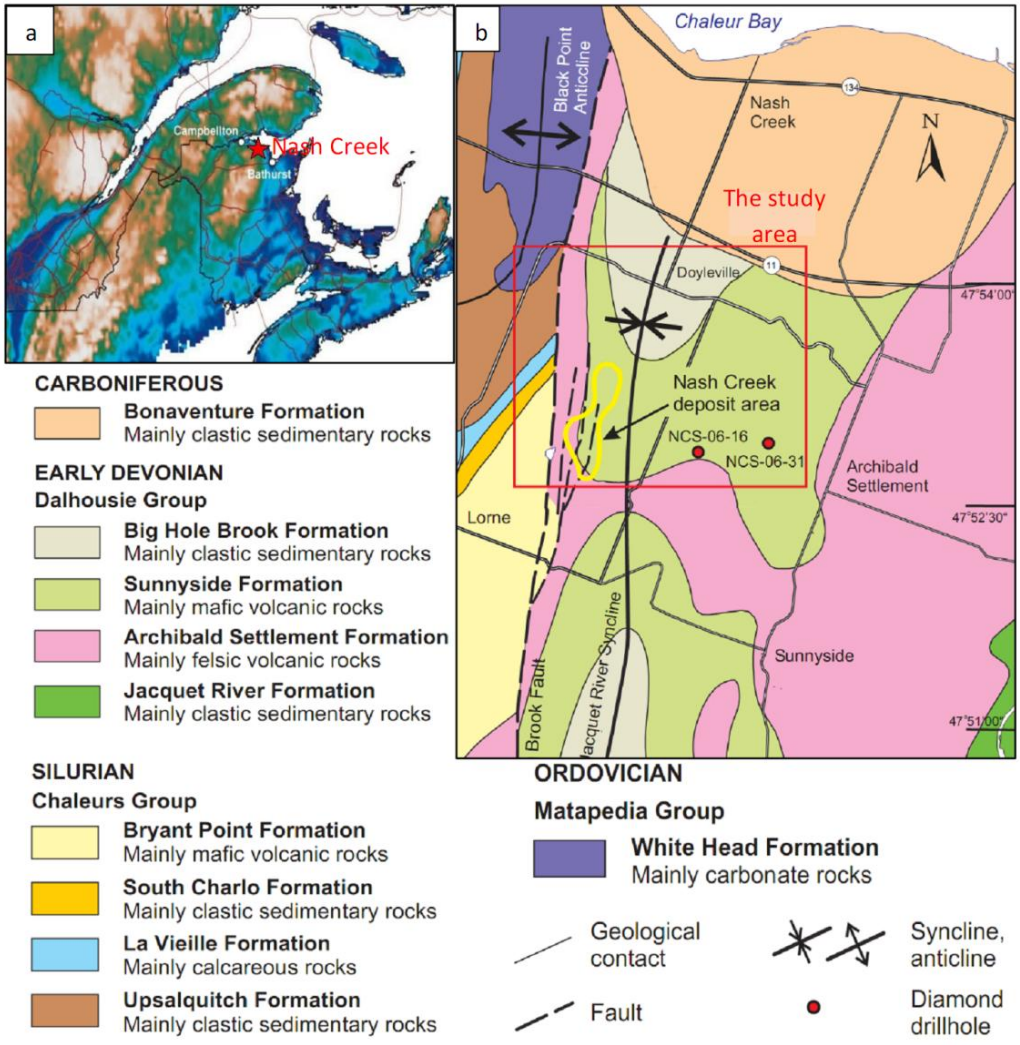

Figure 1 – Approximate location of the Nash Creek area and distribution of the major rock units in the area [17]

The study area location is 5.6 km from NC, with Latitude: 47.876695° East and Longitude: -66.113468° North. The geology of the study area is mostly underlain by the "Lower Devonian" sequence of the "Dalhousie Group", within the CB "Chaleur Bay Synclinorium" belt containing sedimentary and volcanic rocks (breccias, limestones, siltstones, volcanic mafic flows, tuffs, rhyolites, and pillow lavas) [17, 21]. The sedimentary and volcanic rocks were deposited in the half-graben, which is fault-confined to the west [22]. Locally, the prospective "Dalhousie Groups" is covered mainly by Carboniferous rocks. NC sulphide mineralization is hosted within the bi-modal volcanic-sedimentary sequence in the half-graben. In general, the different lithologic units at NC can be divided into three main rock types: mafic rock, felsic rock, and sedimentary rock [23–25].

In general, the NC area comprised of two main zones called the "Hickey Zone", located to the north and the "Hayes Zone", located to the south. Our study area mainly located in "Hickey Zone". The mineralization occurs near to the surface in the "'Hickey Zone". It extended for approximately 2.1 km along strike and interpreted as a series of vertically stacked horizons [26]. Sulphide mineralization deposit intersected by drilling at NC includes sphalerite, galena, pyrite, and rarely chalcopyrite. Ag grades are moderately well correlated with the (Zn-Pb) sulphides. In general, the signature of the mineral deposit distribution indicates an increase in assay from the northern range of the "Hickey Zone" southwards to the "Hayes Zone". Drilling program showed mineralization deposit had been intercepted from the surface to down a maximum depth of around 150 m at the "Hickey Zone" [27].

Materials and Methods.

Theory of geoelectrical survey. Geoelectrical tomography consists of injecting a DC along the survey lines, through two grounded electrodes (A, B) and two other electrodes for measuring the resulting voltage (M, N), as shown in Figure 2. The form of quadrupole A-B-M-N is a variety depends on the order of each electrode and the distance between them. For each form, has a geometrical factor (K), and the apparent resistivity (ρ_a) is calculated from Equation 1. An accessible and convenient means to present the results of the measurements of the survey at a profile is a 2-D "pseudo-section" draw, which is produced by placing each ρ_a measurement at a mid-point of the electrode array (horizontal axis) and a pseudo- depth (vertical axis), as shown in Figure 3 [28].

$$\rho_a = k\frac{\Delta V}{I} \tag{1}$$

where k is a geometrical factor;

$$k = \frac{4\pi}{\frac{1}{r_{MA}} + \frac{1}{\dot{r}_{MA}} - \frac{1}{r_{MB}} - \frac{1}{\dot{r}_{MB}} - \frac{1}{r_{NA}} - \frac{1}{\dot{r}_{NA}} + \frac{1}{r_{NB}} + \frac{1}{\dot{r}_{NB}}},$$

r, $\dot{r}$ are the distances of the real and mirror effect of the ground surface at potential points

(M, N) respectively; ΔV is the measured difference potential at points M and N; I is the applied electric current.

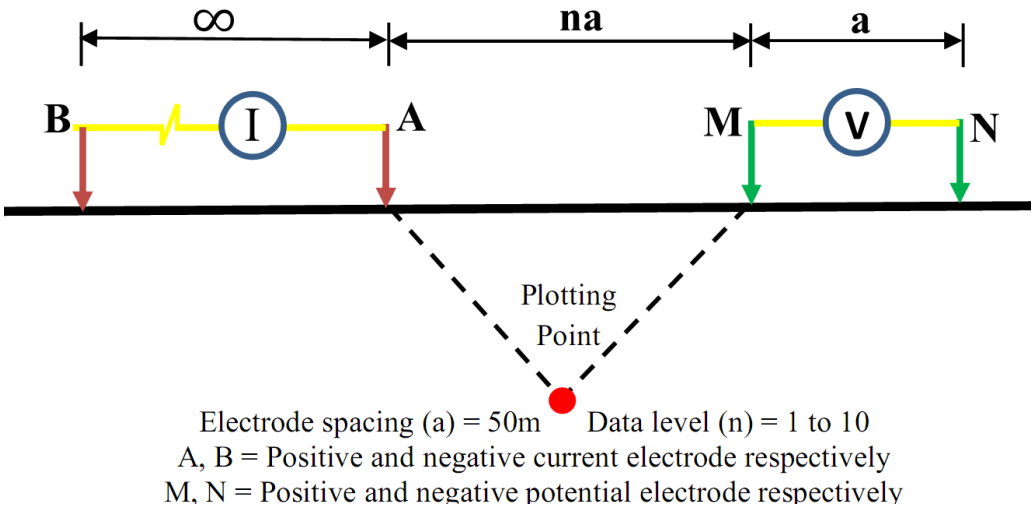

Figure 2 – Pole dipole array system

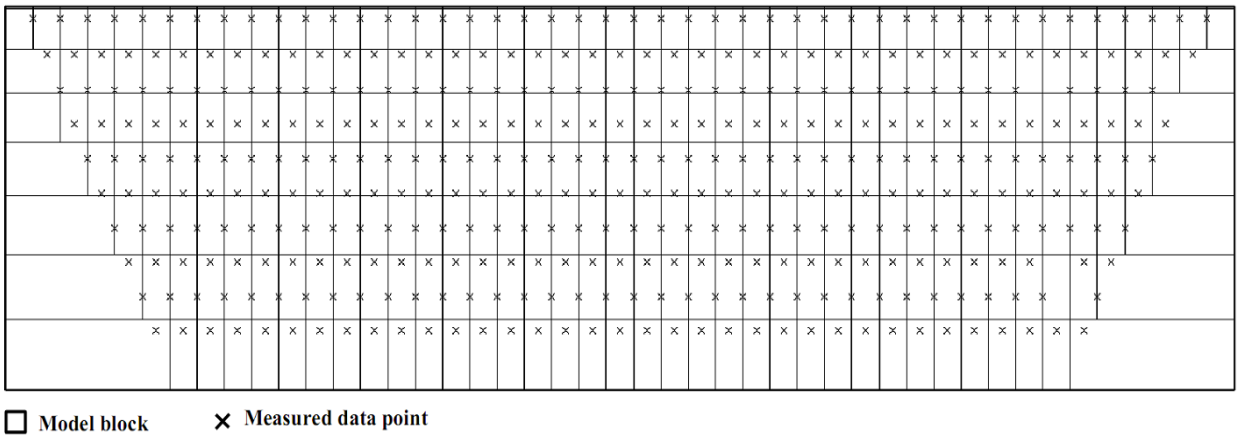

Figure 3 – Arrangement of the model blocks and the measured data points of a pseudo-section

For IP time-domain consists of measuring the potential decay with the time after switch-off the transmitted current to get the apparent chargeability (M_a), which is a measure of the strength of the IP effect, as shown in Figure 4. Therefore, IP measurement of chargeability represents the integrated area under a chosen portion of the decay potential curve (V_t), as shown in Figure 3 and Equation 2 [29]. The potential decay is always measured for positive and negative polarities to cancel DC effects due to self-potential and natural telluric currents.

$$M_a = \frac{1}{V_p} \int_{t_1}^{t_2} V_s(t)dt, \qquad (2)$$

where V_p is the primary voltage, V_s represents secondary voltage, and V_t is the voltage decay with a time interval between t_1 and t_2.

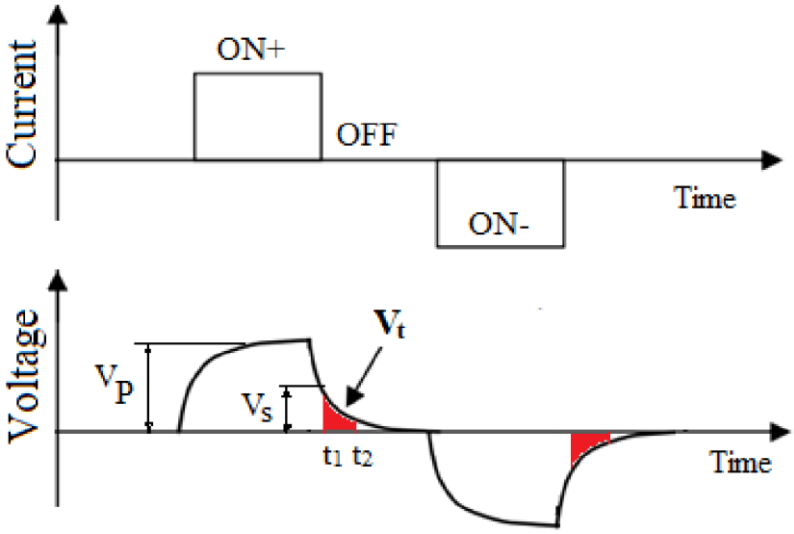

Figure 4 – Time Domain IP Waveform

Field survey and processing. To explore and map the mineralization zones in the study area, the surveying has been conducted by the geoelectrical tomography 2-D survey for a well-cut grid consisting of twelve surface lines (profiles) each around 2 km long, and 300 m apart and the total area around 9.5 km^2, as shown in Figure 5.

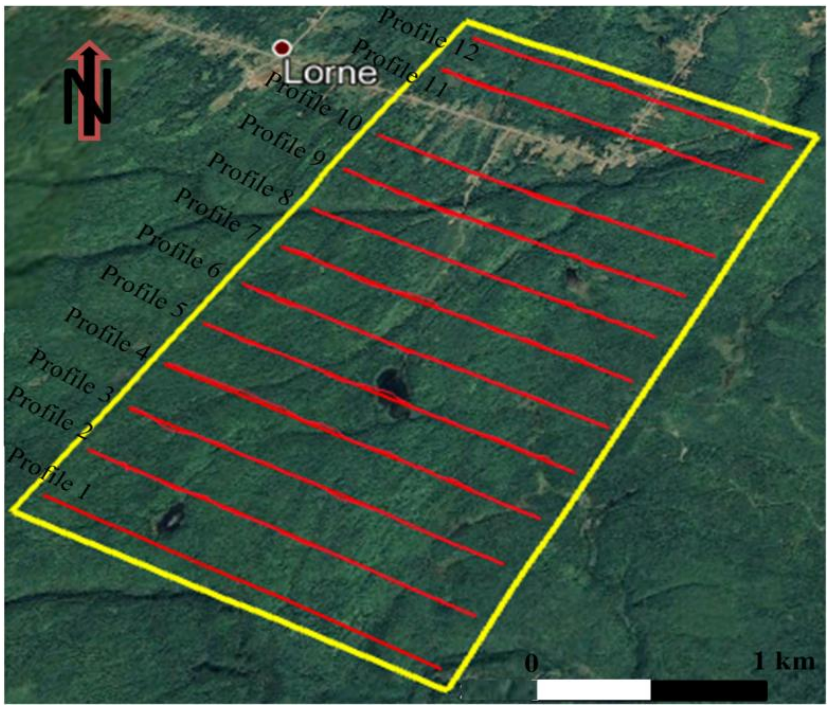

Figure 5 – Map of the survey profiles

The datasets (resistivity and IP values) were acquired using the Iris El-Rec Pro system includes the use of a multi-electrode cable, to which the different number of steel electrodes were used according to the length of the line with pole-dipole electrodes array spaced 50 m apart, and ten levels of data datum as shown in Figure 3. The grid (array spacing) was set to minimize topography alterations. The quadrupole electrode configuration is pole-dipole form was chosen for this surveying

since it is able to a deep depth of exploration and excellent image resolution, combined with a rapid survey speed, in Figure 2 [30–32]. Moreover, a literature search revealed that the pole-dipole form strategy had been applied very successfully in the past investigations of many mineral deposits [31, 33, 34]. For more details about using Pole-dipole array, you can see, for instance, [35–40]. The GPS-data of each electrode of the survey lines was measured by handheld Garmin GPS ± 5 m accuracy and ±10 m accuracy for the elevation, to consider a topographic effect on the inversion processes.

For processing and inversion, the data of each line, we used the RES2DINV inversion modelling ver. 4.8.10 software trial version of the 2-D inversion carried out based on the finite element method developed by [19, 20]. Resistivity and chargeability models were generated by the Robust inversion method based on the least-squares theory. In addition, the inversion was done taking into account adjusting the topography to reduce its effect on the calculated resistivity. The 3-D visualize data modelling was done using Golden Software Voxler 4 trial version.

Results and Discussion. The geoelectrical data were displayed based on resistivity and chargeability values resulted from the inverse process using Res2DInv. According to the inversion results, the resistivity values ranged from (5-1300 Ω.m) and chargeability values ranged from (0-9.5 mV/V). Thus, based on these results and geological information in the study area, the mineralization zones appeared at the medium resistivity and the highest chargeability values because most of the survey lines lie mainly in mafic volcanic rocks, as shown in Figure 1. The zones dominated by high chargeability and low resistivity values point to the occurrence of highly polarized materials. This feature confirms the existence of a zone enriched in sulphide deposits [41].

The previous petrophysical investigations revealed that high-grade sulphides are embedded in pyroclastic units, laterally extensive alteration envelopes while low-grade sulphides are embedded in flow banded Rhyolite units, as shown in Figure 6-a [22]. For that, the mineralization zones appear with moderate resistivity and low chargeability values. The inversion results have been interpreted by correlating with the boreholes logging, as shown in Figure 6-b. According to this correlation in the study area, the sulphide mineralization zones are characterized by moderate resistivity values (150-300 Ω.m) and the highest chargeability values (> 5.5 mV/V). The mineralization zones appear at a depth of around (90-140 m) from the surface. The low chargeability values indicate that most of the sulphide deposit within the explore area is medium to low-grade. This result completely agreed with the geological studies that indicated that the mineral sulphide grade is low in "Hickey Zone", as mentioned above.

In Figures 7-12, the mineralized zone in profile 1 appears at a depth of around 110 m to 130 m from surface, with resistivity values (150-350 Ωm) and chargeability (≈ 5.5 mV/V), as shown in the marked zone with a dashed line.

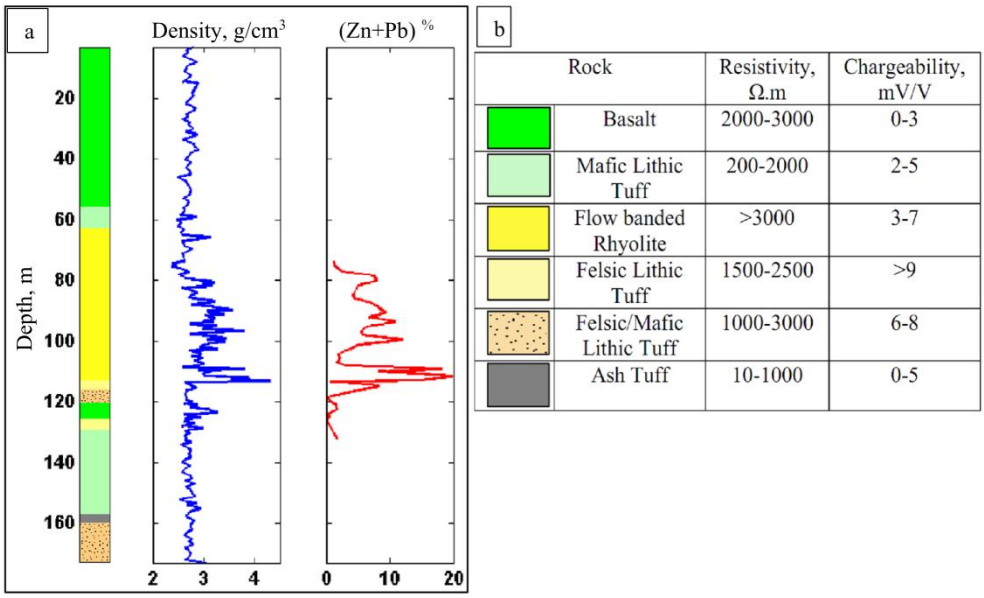

Rock	Resistivity, Ω.m	Chargeability, mV/V
Basalt	2000-3000	0-3
Mafic Lithic Tuff	200-2000	2-5
Flow banded Rhyolite	>3000	3-7
Felsic Lithic Tuff	1500-2500	>9
Felsic/Mafic Lithic Tuff	1000-3000	6-8
Ash Tuff	10-1000	0-5

Figure 6 – a) Density log and assay (%Zn +Pb) data from one example of the boreholes surveyed [22], b) The correlation of the resistivity and chargeability values with boreholes logging

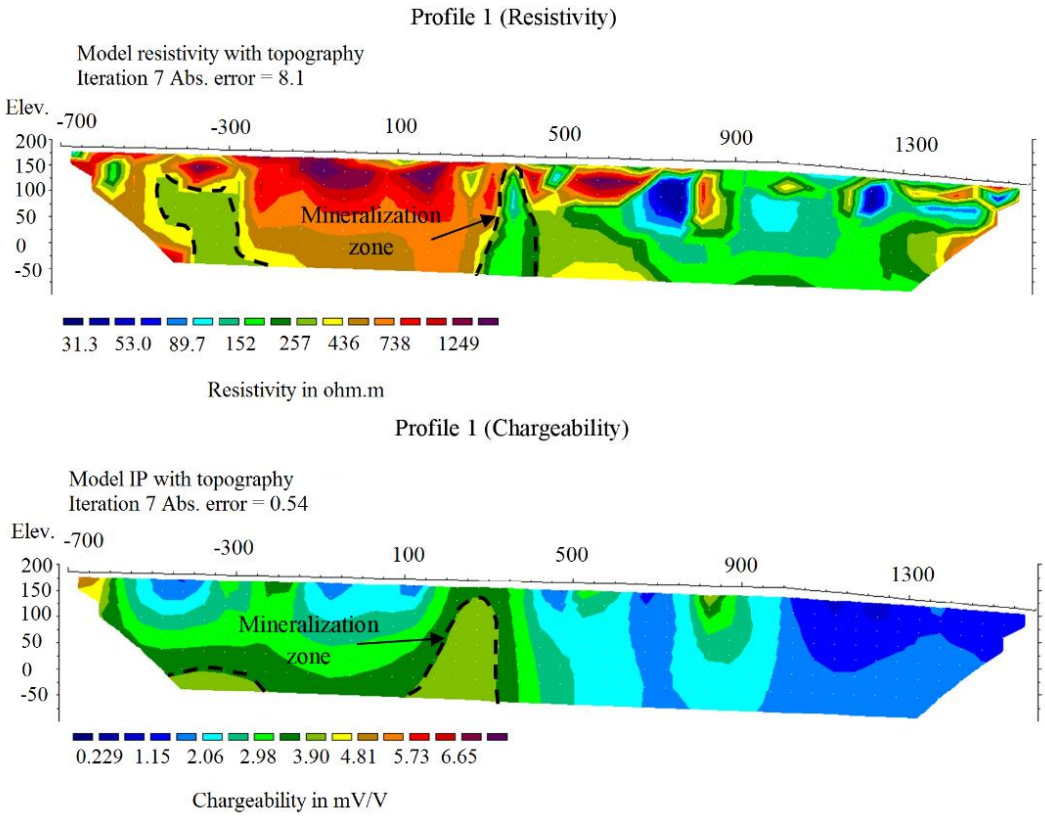

Figure 7 – 2-D inversion results of resistivity and chargeability for profile 1

The low chargeability value in this profile indicates that the sulphide deposit is a low grade. In addition, the short of the mineralization zone extent indicates that the deposit occurrence is weak along to this profile. From profile 2 to profile 4, the mineralization zone appears at a shallow depth, approximately near to the surface with a low grade and a short extent along to the profiles. In contrast to profiles 5 and

6, the mineralization zone appears at a relatively higher depth and with higher grade and extent than previous profiles.

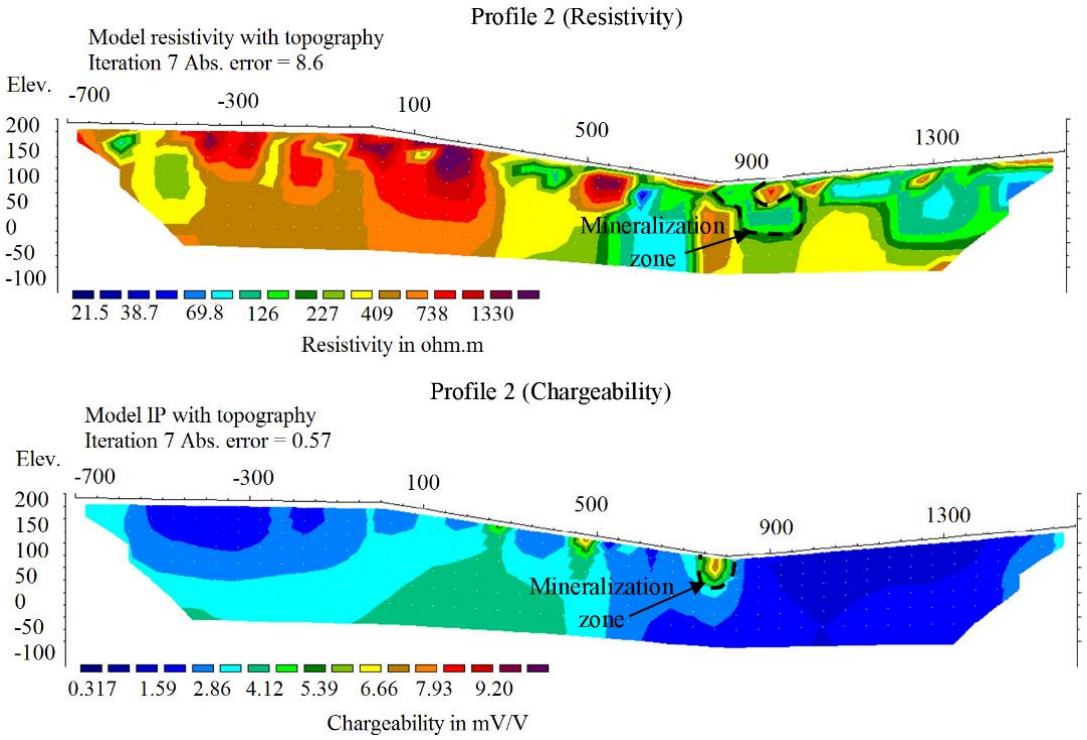

Figure 8 – 2-D inversion results of resistivity and chargeability for profile 2

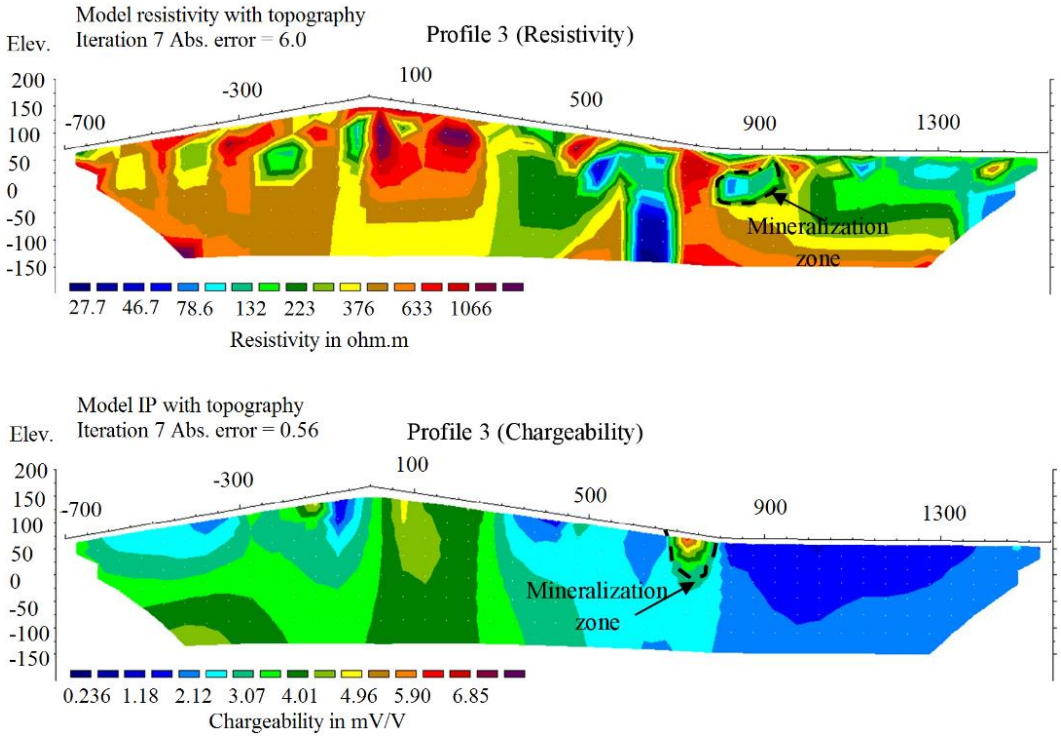

Figure 9 – 2-D inversion results of resistivity and chargeability for profile 3

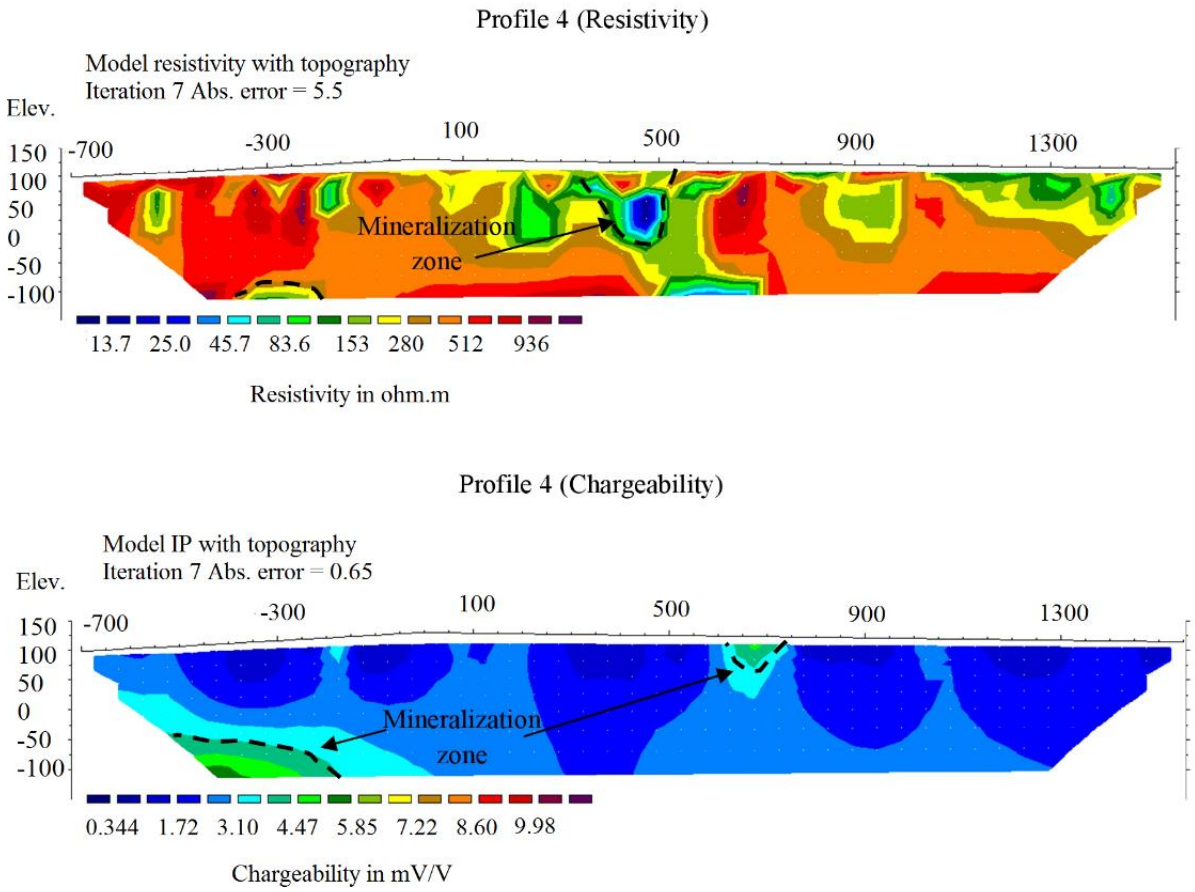

Figure 10 – 2-D inversion results of resistivity and chargeability for profile 4

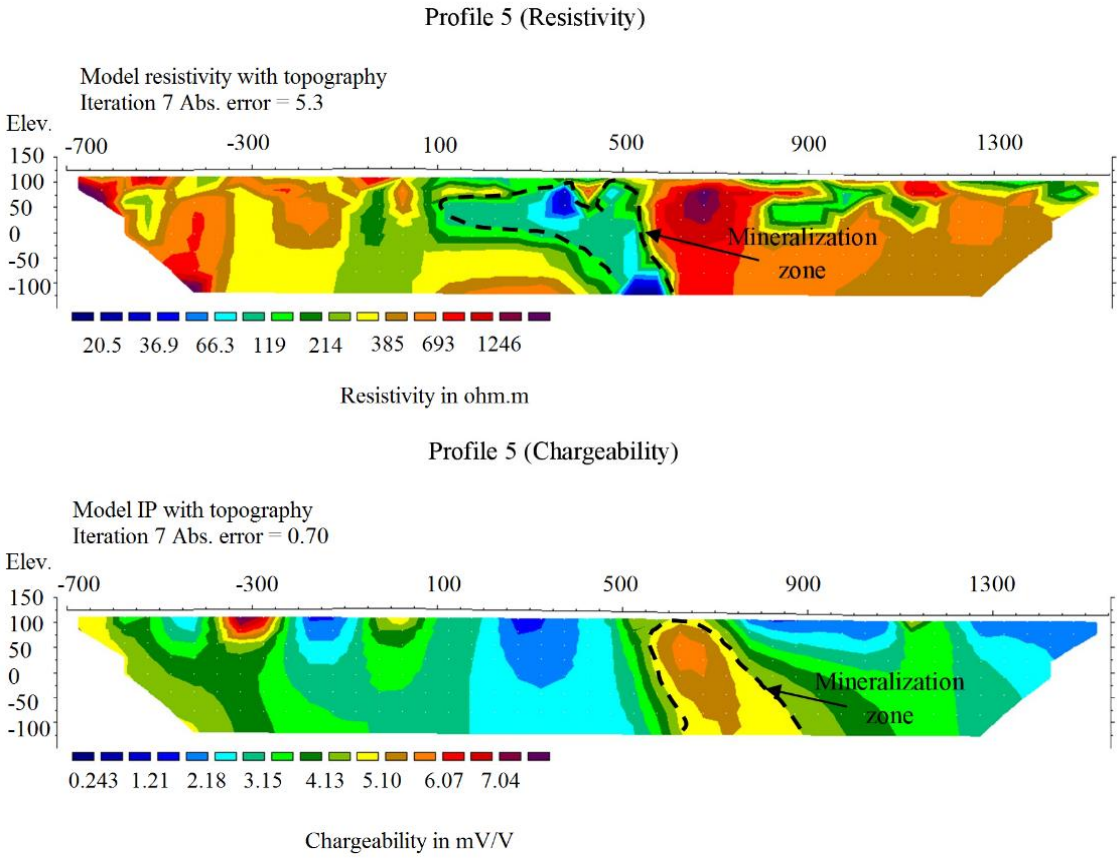

Figure 11 – 2-D inversion results of resistivity and chargeability for profile 5.

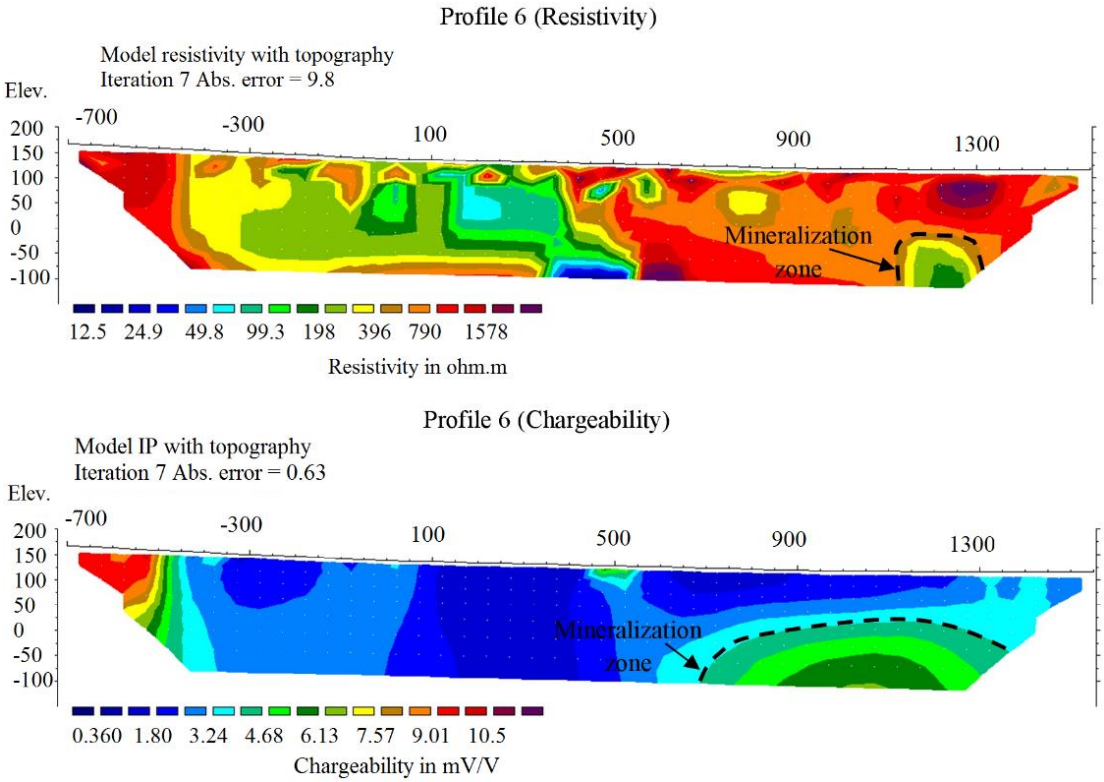

Figure 12 – 2-D inversion results of resistivity and chargeability for profile 6

In Figures 13-18, the mineralization zone appears again at a relatively shallow depth and with a low grade and a medium extent along to profiles 7 to 9. While in profiles 10 to 12, the mineralization zone appears at a relatively higher depth and with higher grade and extent than previous profiles. In general, the boundaries around the mineralized zones in the chargeability profiles are more clear than the resistivity profiles, because of the ability of the IP method for mineral discrimination than other geophysical methods [42–44].

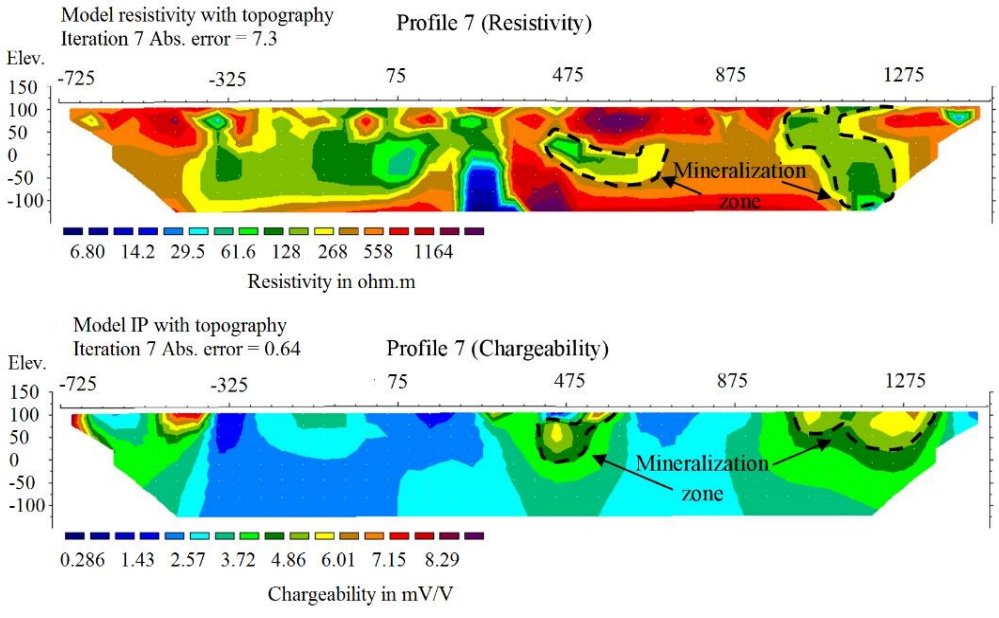

Figure 13 – 2-D inversion results of resistivity and chargeability for profile 7

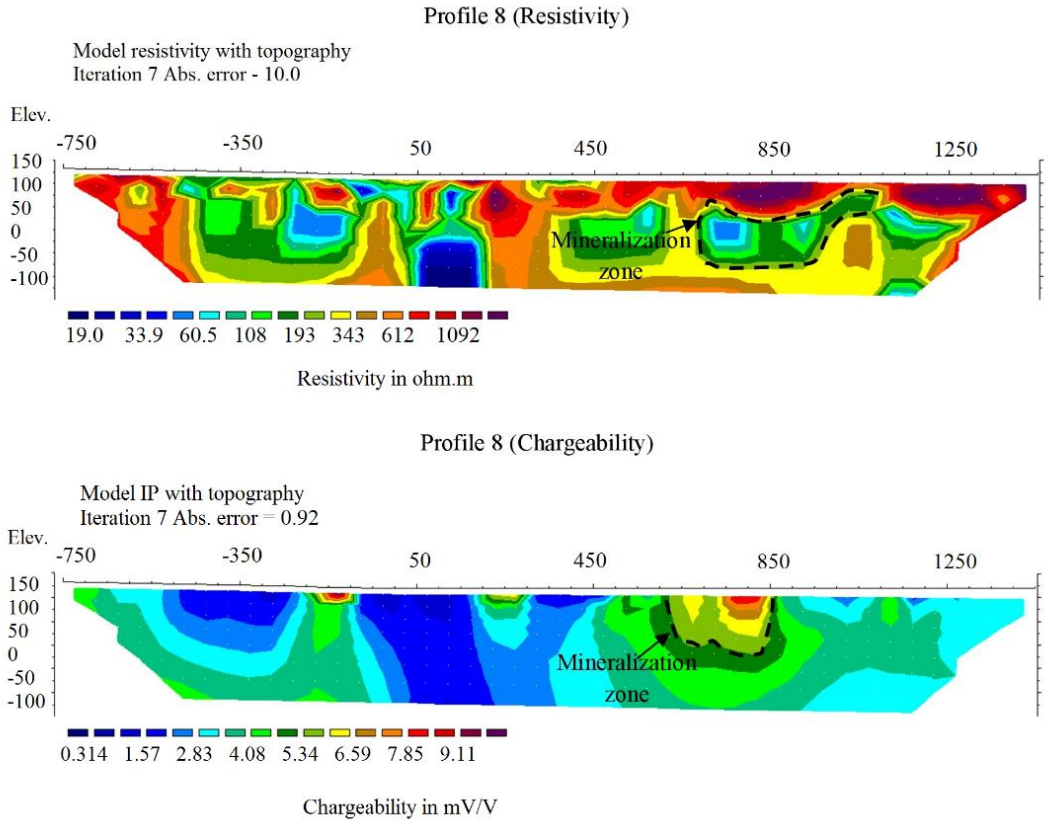

Figure 14 – 2-D inversion results of resistivity and chargeability for profile 8

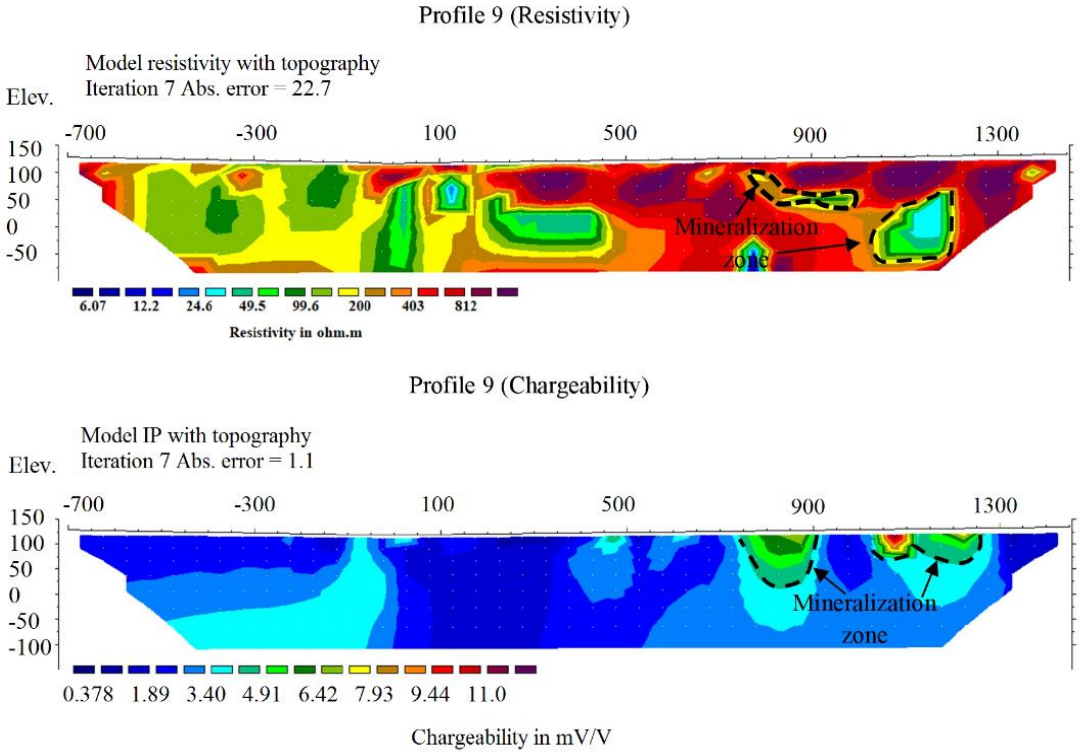

Figure 15 – 2-D inversion results of resistivity and chargeability for profile 9

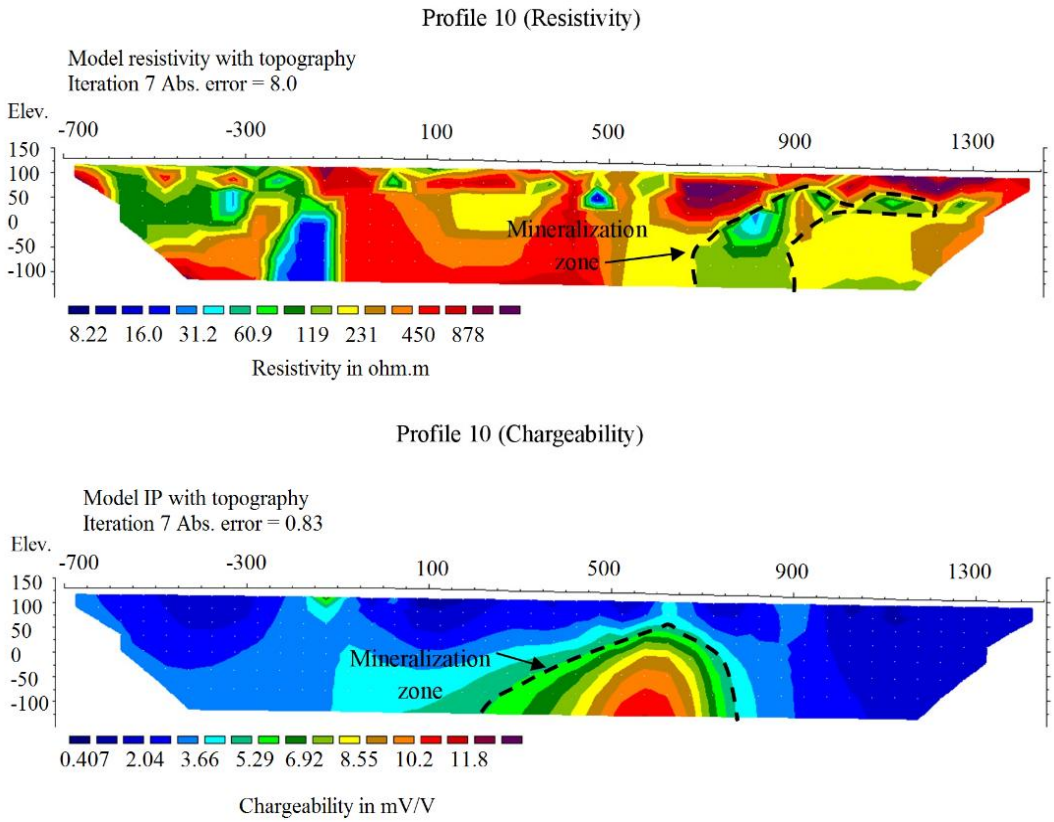

Figure 16 – 2-D inversion results of resistivity and chargeability for profile 10

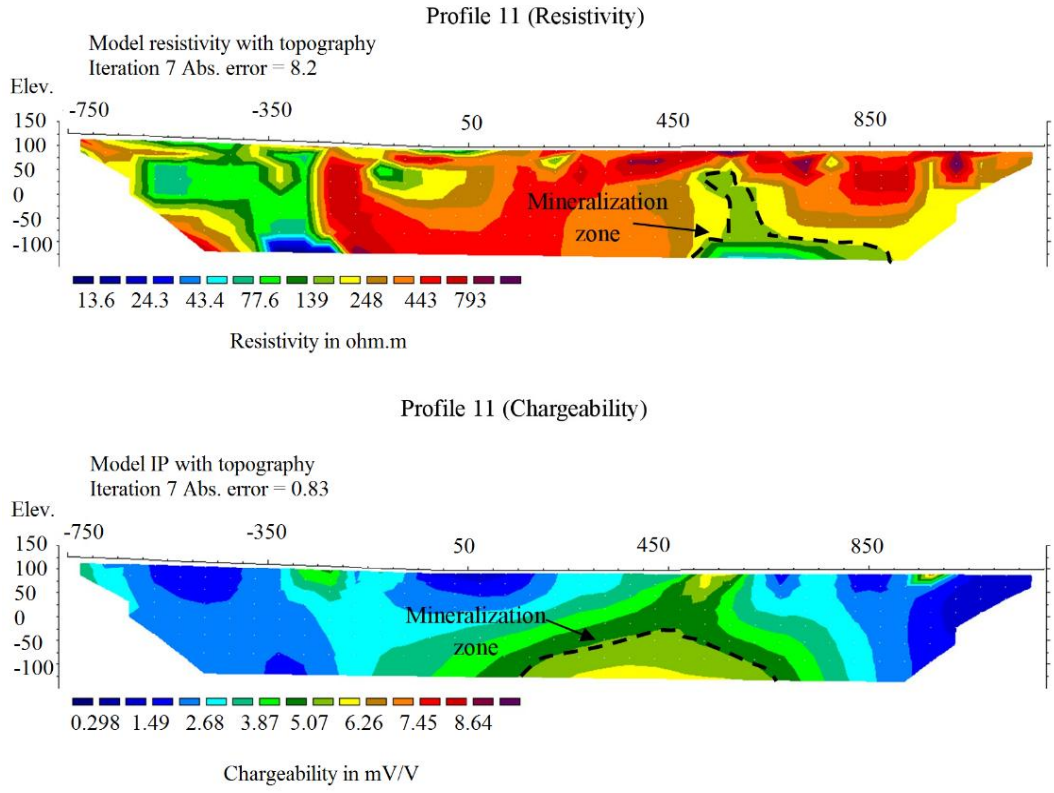

Figure 17 – 2-D inversion results of resistivity and chargeability for profile 11

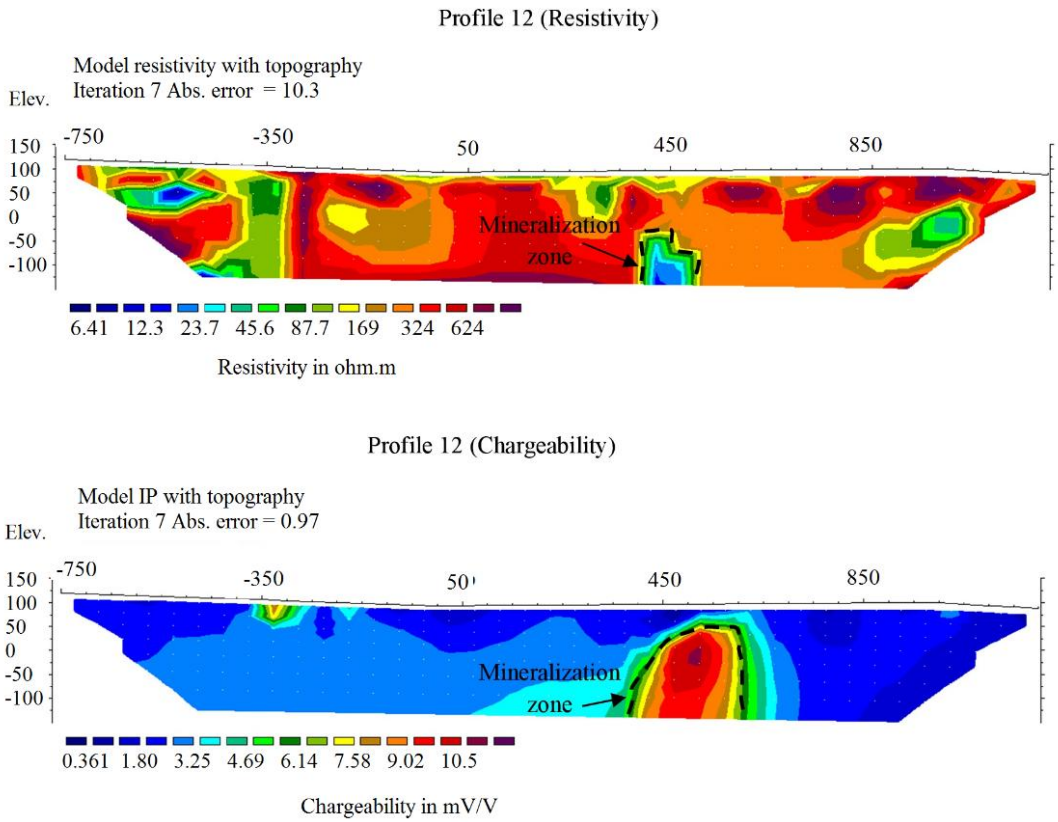

Figure 18 – 2-D inversion results of resistivity and chargeability for profile 12

The results of 2-D inversion were visualized in a 3-D model using Golden Software Voxler 4 visualization modelling, to remove the ambiguity somewhat. The cut-off values of the model are (150-300 Ω.m) and (> 5.5 mV/V) for the resistivity and chargeability, respectively. The model clearly reveals that three main zones of sulphide mineralization are present in the exploration area, as shown in Figure 19. The total volume of these zones is 3536250 m^3 calculated by the Voxler software. The average density of the NC (Zn-Pb-Ag) sulphide ore is approximately 3.0 g/cm^3, according to the result of the petrophysical study done by [22]. From the volume and density of the sulphide ore, the predicted geological reserve of the sulphide ore is 10.61 million tons.

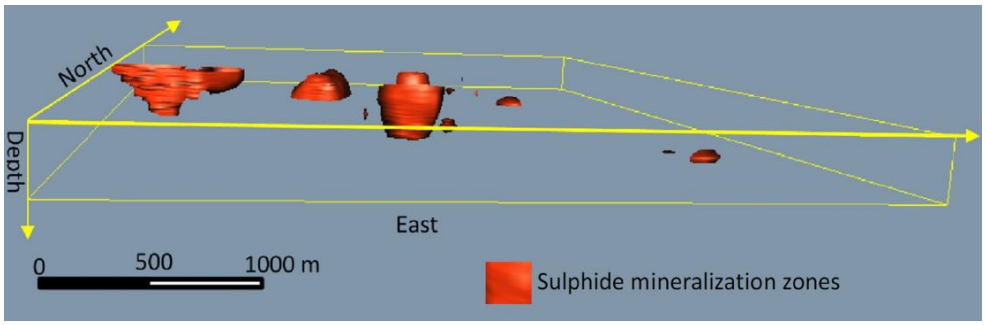

Figure 19 – 3-D visualization model of the occurrence of sulphide mineralization zones in the exploration area

Conclusions. The geoelectrical tomography survey and 2-D inversion result revealed that the underground resistivity and chargeability values in the exploration area have a range of (5 to 1300 Ωm) and (0-9.5 mV/V) respectively. The sulphide mineralization zones in the exploration area are characterized by moderate resistivity values (150-300 Ωm) and moderate to low chargeability values (> 5.5 mV/V). The 3-D visualization model clearly reveals that three main zones of sulphide mineralization are present in the exploration area. The predicted geological reserve of the sulphide ore in exploration area was calculated. The inverted models revealed a good agreement with the existing geological features in the exploration area. The study recommends that if pre-existing information regarding the geological environment is available, then geoelectrical tomography data (resistivity and changeability) can be a helpful and fascinating mixture for mineral exploration.

REFERENCES

1. J. Martinez, J. Rey, S. Sandoval, Hidalgo, R. Mendoza, Geophysical Prospecting Using ERT and IP Techniques to Locate Galena Veins. Remote Sens. 11, 2923 (2019). https://doi.org/10.3390/rs11242923

2. S. Uhlemann, J. Chambers, W. Falck, A. Tirado Alonso, J. Fernández González, A. de Gea, Applying electrical resistivity tomography in ornamental stone mining: challenges and solutions. Minerals. 8, 491 (2018). https://doi.org/10.3390/min8110491

3. S. A. Sultan, S. A. Mansour, F. M. Santos, A. S. Helaly, Geophysical exploration for gold and associated minerals, case study: Wadi El Beida area, South Eastern Desert, Egypt. J. Geophys. Eng. 6, 345-356 (2009). https://doi.org/10.1088/1742-132/6/4/002

4. A. R. Heritiana, R. Riva, R. Ralay, R. Boni, Evaluation of flake graphite ore using self-potential (SP), electrical resistivity tomography (ERT) and induced polarization (IP) methods in east coast of Madagascar. J. Appl. Geophys. (2019). https://doi.org/10.1016/j.jappgeo.2019.07.001

5. C. A. Moreira, E. G. Dos Santos, L. M. Ilha, R. Paes, Recognition of Sulfides Zones in Marble Mine Through Comparative Analysis of Electrical Tomography Arrangements. Pure Appl. Geophys. 176, 4907-4920 (2019). https://doi.org/10.1007/s00024-019-02243-y

6. M. Ali, S. Sun, W. Qian, A. D. Bohari, D. Claire, Y. Zhang, Application of Resistivity Method for Mining Tailings Site Selection in Karst Regions. E3S Web Conf. 144, 1002 (2020). https://doi.org/10.1051/e3sconf/202014401002

7. J. M. Reynolds, An introduction to applied and environmental geophysics, John Wiley & Sons, (2011)

8. G. Zhang, Q.-T. Lü, P.-R. Lin, G.-B. Zhang, Electrode array and data density effects in 3D induced polarization tomography and applications for mineral exploration. Arab. J. Geosci. 12, 221 (2019). https://doi.org/10.1007/s12517-019-4341-0

9. S. R. Mashhadi, H. Ramazi, The application of resistivity and induced polarization methods in identification of skarn alteration haloes: A case study in the Qale-Alimoradkhan Area. J. Environ. Eng. Geophys. 23, 363-368 (2018)

10. M. A. Hussein, S. S. Imbaby, A. R. Ibrahim, Panel Width Affected by Rock Mass Classifications (Abu-Tartur Phosphate Mines). Accept. under Publ. JES. 41 (2013)

11. W. H. Pelton, S. H. Ward, P. G. Hallof, W. R. Sill, P. H. Nelson, Mineral discrimination and removal of inductive coupling with multifrequency IP. Geophysics. 43, 588-609 (1978). https://doi.org/10.1190/1.1440839

12. P. H. Nelson, G. D. Van Voorhis, Estimation of sulfide content from induced polarization data. Geophysics. 48, 62-75 (1983). https://doi.org/10.1190/1.1441408

13. G. Gurin, K. Titov, Y. Ilyin, Induced Polarization of Rocks Containing Metallic Particles: Evidence of Passivation Effect. Geophys. Res. Lett. 46, 670-677 (2019). https://doi.org/10.1029/2018GL080107

14. C. L. Bérubé, G. R. Olivo, M. Chouteau, S. Perrouty, Mineralogical and textural controls on spectral induced polarization signatures of the Canadian Malartic gold deposit: Applications to mineral exploration. Geophysics. 84, B135--B151 (2019). https://doi.org/10.1190/geo2018-0404.1

15. D. J. Vaughan, Sulfide mineralogy and geochemistry: introduction and overview. Rev. Mineral. Geochemistry. 61, 1-5 (2006). https://doi.org/10.2138/rmg.2006.61.1

16. C. Moreno, R. Sáez, F. González, G. Almodóvar, M. Toscano, G. Playford, A. Alansari, S. Rziki, A. Bajddi, Age and depositional environment of the Draa Sfar massive sulfide deposit, Morocco. Miner. Depos. 43, 891 (2008). https://doi.org/10.1007/s00126-008-0199-x

17. J. A. Walker, Stratigraphy and lithogeochemistry of Early Devonian volcano-sedimentary rocks hosting the Nash Creek Zn-Pb-Ag Deposit, northern New Brunswick (pp. 52-97). Geol. Investig. New Brunswick 2009. Ed. by G.L. Martin. New Brunswick Dep. Nat. Resour. Lands, Miner. Pet. Div. Miner. Resour. Rep., 52-97 (2010)

18. M. A. Hussein, A. R. Ibrahim, S. S. Imbaby, Load calculations and selection of the powered supports based on rock mass classification and other formulae for Abu-Tartur longwall phosphate mining conditions. J. Eng. Sci. 41, 1728-1742 (2013)

19. T. Dahlin, 2D resistivity surveying for environmental and engineering applications. First Break. 14, 275-283 (1996).

https://doi.org/10.3997/1365-2397.1996014

20. M. H. Loke, J. E. Chambers, D. F. Rucker, O. Kuras, P. B. Wilkinson, Recent developments in the direct-current geoelectrical imaging method. J. Appl. Geophys. 95, 135-156 (2013). https://doi.org/10.1016/j.jappgeo.2013.02.017

21. D. F. Brown, Technical report on mineral resource estimate. Nash Creek Proj. Restigouche County, New Brunswick, Canada, 1-190 (2007)

22. B. Milkereit, W. Qian, H. Ugalde, E. Bongajum, M. Gräber, Geophysical Imaging of a" Blind. Zn-Pb-Ag Depos. EAGE Expand. Abstr. Rome, 9-12 (2008). https://doi.org/10.3997/2214-4609.20147628

23. E. Bongajum, B. Milkereit, J. Huang, Building 3D stochastic exploration models from borehole geophysical and petrophysical data: A case study. Can. J. Explor. Geophys. 38, 40-50 (2013)

24. M. A. Hussein, A. R. Ibrahim, S. S. Imbaby, Application of the Rock Mass Classification Systems to Pillar Design in Longwall Mining for Abu-Tartur Longwall Phosphate Mining Conditions. J. Eng. Sci. 41, (2013)

25. A. D. Bohari, M. Harouna, A. Mosaad, Geochemistry of Sandstone Type Uranium Deposit in Tarat Formation from Tim-Mersoi Basin in Northern Niger (West Africa): Implication on Provenance, Paleo-Redox and Tectonic Setting. J. Geosci. Environ. Prot. 6, 185 (2018). https://doi.org/10.4236/gep.2018.68014

26. I. R. Annesley, C. Cutforth, D. Billard, R. T. Kusmirski, K. Wasyliuk, T. Bogdan, K. Sweet, C. Ludwig, D. R. Lentz, K. G. Thorne, others, in International Applied Geochemistry Symposium, 40, 421(2009)

27. P. James, F. Barr, "Technical Report and Updated Mineral Resource Estimate on the Nash Creek Project, New Brunswick, Canada" (2018)

28. M. H. Loke, R. D. Barker, Rapid least-squares inversion of apparent resistivity pseudosections by a quasi-Newton method. Geophys. Prospect. 44, 131-152 (1996). https://doi.org/10.1111/j.1365-2478.1996.tb00142.x

29. H. O. Seigel, Mathematical formulation and type curves for induced polarization. Geophysics. 24, 547-565 (1959). https://doi.org/10.1190/1.1438625

30. D. W. Oldenburg, Y. Li, Estimating depth of investigation in dc resistivity and IP surveys. Geophysics. 64, 403-416 (1999). https://doi.org/10.1190/1.1444545

31. S. Tavakoli, T. E. Bauer, T. M. Rasmussen, P. Weihed, S.-Å. Elming, Deep massive sulphide exploration using 2D and 3D geoelectrical and induced polarization data in Skellefte mining district, northern Sweden. Geophys. Prospect. 64, 1602-1619 (2016). https://doi.org/10.1111/1365-2478.12363

32. T. Dahlin, B. Zhou, A numerical comparison of 2D resistivity imaging with 10 electrode arrays. Geophys. Prospect. 52, 379-398 (2004). https://doi.org/10.1111/j.1365-2478.2004.00423.x

33. R. D. Ogilvy, Down-hole IP surveys applied to off-hole mineral exploration-some design considerations. Geoexploration. 22, 59-73 (1984). https://doi.org/10.1016/0016-7142(84)90006-1

34. J. Bernard, O. Leite, F. Vermeersch, I. Instruments, F. Orleans, Multi-electrode resistivity imaging for environmental and mining applications. IRIS Instruments, Orleans (2006)

35. M. H. Loke, Tutorial : 2-D and 3-D electrical imaging surveys. Geotomo Software, Malaysia, 127 (2014)

36. E. H. Eloranta, A Comparison between Mise-à-la-Masse anomalies obtained by pole-pole and pole-dipole electrode configurations. Geoexploration. 23, 471-481 (1985). https://doi.org/10.1016/0016-7142(85)90074-2

37. S. Chandra, V. A. Rao, V. S. Singh, A combined approach of Schlumberger and axial pole--dipole configurations for groundwater exploration in hard-rock areas. Curr. Sci., 1437-1443 (2004)

38. J. E. Nyquist, M. J. S. Roth, Improved 3D pole-dipole resistivity surveys using radial measurement pairs. Geophys. Res. Lett. 32 (2005). https://doi.org/10.1029/2005GL024153

39. A. A. Hassan, E. H. Kadhim, M. T. Ahmed, Performance of Various Electrical Resistivity Configurations for Detecting Buried Tunnels Using 2D Electrical Resistivity Tomography Modelling. DIYALA J. Eng. Sci. 11, 14-21 (2018). https://doi.org/10.24237/djes.2018.11303

40. N. Usman, K. Abdullah, M. Nawawi, Investigating the performance of combined resistivity model using different electrode arrays configuration. Arab. J. Geosci. 12, 125 (2019). https://doi.org/10.1007/s12517-018-4192-0

41. C. A. Moreira, S. M. Lopes, C. Schweig, A. da Rosa Seixas, Geoelectrical prospection of disseminated sulfide mineral occurrences in Camaquã sedimentary basin, Rio Grande do Sul state, Brazil. Brazilian J. Geophys. 30 (2012). https://doi.org/10.22564/rbgf.v30i2.90

42. G. Gurin, K. Titov, Y. Ilyin, A. Tarasov, Induced polarization of disseminated electronically conductive minerals: a semi-empirical model. Geophys. J. Int. 200, 1555-1565 (2015). https://doi.org/10.1093/gji/ggu490

43. G. Gurin, A. Tarasov, Y. Ilyin, K. Titov, Time domain spectral induced polarization of disseminated electronic conductors: Laboratory data analysis through the Debye decomposition approach. J. Appl. Geophys. 98, 44-53 (2013). https://doi.org/10.1016/j.jappgeo.2013.07.008

44. A. Revil, N. Florsch, D. Mao, Induced polarization response of porous media with metallic particles -Part 1: A theory for disseminated semiconductors. Geophysics. 80, D525-D538 (2015). https://doi.org/10.1190/geo2014-0577.1